NATIONAL RADIO ASTRONOMY OBSERVATORY
Green Bank, West Virginia

Electronics Division Internal Report No. 36

THE CHARACTERISTICS OF THE NRAO 85-FT. TELESCOPES
AT 2.07 CM WAVELENGTH

J.W.M. Baars and P.G. Mezger

OCTOBER 1964

THE CHARACTERISTICS OF THE NRAO 85-FT. TELESCOPES
AT 2.07 CM WAVELENGTH

J.W.M. Baars and P.G. Mezger

1. Introduction

These measurements are part of the program which has been initiated in order to test the NRAO telescopes under extreme operating conditions. "Extreme conditions" mean that the telescope is operated at a wavelength where there is already a substantial reduction in gain and aperture efficiency due to the RMS deflection $\sqrt{\bar{d}^2}$ of the reflector. Most of the formulas used in the following sections have been discussed or derived in two earlier papers, [1], [2].

The measurements were started (on March 15, 1964) using a superheterodyne receiver which was borrowed from the Naval Research Laboratory in Washington, D. C. This radiometer received both signal and image frequency. The L.O. was tuned to 14.5 GHz. The 85(I)-ft. telescope turned out to be still a very useful instrument at this short wavelength. It, therefore, was decided to start some radio astronomical observations, the result of which will be communicated elsewhere. At the end of the measuring period the setting of the reflector of the 85(II)-ft. telescope was just completed. The receiver was then mounted for six days (beginning on May 5) in the new telescope and the most important characteristics of this telescope were also measured.

For these measurements a horn feed was used whose edge taper (free space taper not included) is -14 dB as compared to a taper of -16 dB of those feeds normally used at NRAO. The path difference Δ between the ray from the focal point to the edge and that to the vertex of a paraboloid is given by

$$\Delta = \frac{D}{4} \, tg \, \frac{\Theta_o}{2} \, , \text{ where } \Theta_o \text{ is the aperture angle.}$$

The space attenuation A of a ray under an angle Θ with the central ray is given by the relation

$$A = 20 \log \sec^2 \frac{\Theta}{2} \, , \text{ in dB.}$$

For $\Theta_o = 60°$ we arrive at a free space taper for the edge ray 2.5 dB larger than that for the central ray. All antenna measurements have been done with the E-plane of the feed oriented in N-S direction.

2. Beam Efficiency and Aperture Efficiency at $\lambda = 2.07$ cm

The antenna temperature of Taurus A, reduced to zenith distance $z = 0°$ and corrected for atmospheric extinction and polarization, is

(1) $T_{AI}(Tau) = 13.16°K$

The corresponding antenna temperature measured with the 85(II)-ft. telescope is

(2) $T_{AII}(Tau) = 1.03 \, T_{AI}(Tau)$

The flux density of Taurus, as obtained from our analysis of the spectra of the strongest nonthermal sources [4] is

(3) $S_{14.5 \text{ GHz}}(Tau) = 510.10^{-26} \text{ W/m}^2\text{Hz}$

The HPBW of the 85(I)-ft. telescope, as measured with the planets Venus and Jupiter, is

(4) θ_{AI} = 3.35 min of arc

This value is also obtained using Wade's semiempirical formula. Taurus has an approximately gaussian distribution with minimum and maximum HPW's θ_s" = 2.6' and θ_s' = 4.2', respectively. With the correction factors

(5) $\Omega_s' = 1.133\ \theta_s'\ \theta_s"\ [1 + \theta_s'^2/\theta_A^2]^{-1/2}\ [1 + \theta_s"^2/\theta_A^2]^{-1/2}$

$\Omega_s/\Omega_s' = [1 + \theta_s'^2/\theta_A^2]^{1/2}\ [1 + \theta_s"^2/\theta_A^2]^{1/2}$

valid for gaussian distributions [3] and a circular main beam with main beam solid angle $\Omega_m = 1.133\ \theta_A^2$ one obtains the relations

(6a) $S_\nu = \dfrac{2kT_A}{\lambda^2\eta_B}\ \Omega_m\ \dfrac{\Omega_s}{\Omega_s'}$

(6b) $S_\nu = \dfrac{2kT_A}{A}\ \dfrac{\Omega_s}{\Omega_s'}$

Integrating the antenna temperature over the main beam area yields the formula ([2] eq. 2).

(7) $S_\nu = \dfrac{2k}{\lambda^2\eta_B}\ \displaystyle\int\!\!\int_{\substack{main \\ region}} T_A\ (\xi,\eta)\ d\xi\ d\eta$

With the numerical value $\iint T_A(\xi,\eta)\, d\xi\, d\eta = 319°K$ (min of arc)^2 and the above given values one finds

(8a)
(8b)

$$\eta_B = \begin{cases} 0.342 & (\text{eq. } 7) \\ 0.358 & (\text{eq. } 6a) \end{cases}$$

With the relation between aperture efficiency and beam efficiency

(9) $$\eta_A = 0.76\ \eta_B$$

we find for the aperture efficiency

(10)

$\eta_A =$	85(I)-ft.	85(II)-ft.	Using equation
	0.260	0.268	8a; 9
	0.273	0.281	8b; 9
	0.279	0.287	6b and $\eta_A = A/A_g$

3. The RMS Reflector Deviations

The best values for the aperture efficiency of the 85(I)-ft. telescope at various wavelengths are given in the following table.

Table 1

Wavelength	Aperture efficiency	Estimated error
21.1 cm	0.58	± 10%
10 cm	0.52	± 15%
6 cm	0.51	± 10%
3.95 cm	0.34	± 15%
2.07 cm	0.27	± 10%

The measured and weighted RMS reflector deviations are given in the following table (compare also [1]).

Table 2

	$z = 0°$	$z = 90°$
RMS reflector deviation from photogrammetric measurement	3.16	5.71
Weighted for feed taper	2.75	4.17
Effective RMS reflector deviation	1.75 $\begin{cases} 85(I)\text{-ft.} \\ 85(II)\text{-ft.} \end{cases}$	1.92 (85(I)-ft.) 1.83 (85(II)-ft.)
RMS reflector deviation of the 85(II) -foot telescope as measured by Wade	2.14	

The aperture efficiency decreases with increasing RMS phase error

$\sqrt{\overline{\delta^2}}$ according to

$$(11) \qquad \eta_A(\lambda) = \eta_{A_o} \exp\{-\overline{\delta^2}\}$$

with $\qquad \overline{\delta^2} = 16\pi^2 \dfrac{\overline{d^2}}{\lambda^2}$

η_{A_o} is the aperture efficiency of the undisturbed reflector. It is obtained by plotting log (η_A) over $1/\lambda^2$ and calculating the best fitting straight line through these points. We found

$$(12) \qquad \eta_{A_o} = 0.59$$

In the same way the effective reflector deviation can be found which led to the value $\sqrt{\overline{d^2}}$ = 1.75 mm in Table 2.

The aperture efficiency as a function of wavelength has been calculated using eq. (11), (12) and the RMS deflections at z = 0° as given in Table 2. It is quite obvious that the photogrammetric survey yields a much too high RMS deviation, whereas Wade's measurement of the 85(II)-ft. reflector is in better agreement with the effective RMS deviation determined by purely high frequency measurements*.

If the telescopes are tilted from zenith to horizon the aperture efficiency decreases. This is a very general feature of most radio telescopes, since their reflectors have been in most cases set at zenith position.

The change in aperture efficiency can be determined by measuring point sources at various hour angles (and hence at various elevation angles). The antenna temperature of a point source is directly proportional to the aperture efficiency apart from the influence of atmospheric extinction. If T_A is the antenna temperature measured at $z = 0°$, then the antenna temperature at any zenith distance z is

$$(13) \qquad T_A(z) = T_A p^{F(z)}$$

with p the zenith extinction coefficient; $F(z)$ the air mass function.

Adopting $\log (p_{14.5 \text{ GHz}}) = -0.001$ and $F(z = 80°) = 5.6$, one obtains $p^{F(z)} = 0.9$. That means that the atmospheric extinction causes at $z = 80°$ and for $\lambda = 2.07$ cm an apparent change in the aperture efficiency of 10%. The measured values have, therefore, to be corrected for extinction. The result of our measurements is presented in the form of two curves in fig. 1. The aperture efficiency changes between zenith and horizon position by 40% (85(I)-ft.) and 10% (85(II)-ft.), respectively.

This gain change could be caused by either a systematic defocusing of the feed or by an increase in the RMS reflector deviation. If d is the effective RMS deviation at zenith and $d + \Delta d$ is the effective RMS deviation at zenith distance z, then

$$\frac{\eta_A(z)}{\eta_A(0)} = \exp \left\{ - 16\pi^2 \, \frac{\Delta d(2d + \Delta d)}{\lambda^2} \right\}$$

and for $\Delta d \ll d$,

$$(14) \qquad \Delta d = \frac{\lambda^2}{2d} \, \frac{\log [\eta_A(0)/\eta_A(z)]}{16\pi^2}$$

Inserting in this equation d = 1.75 mm and $\log\left[\dfrac{\eta_A(0)}{\eta_A(90°)}\right] = 0.224$ for the

85(I)-ft. and 0.063 for the 85(II)-ft. telescope, one obtains Δd = 0.17

and 0.078, respectively, for the increase in the RMS reflector deviations

between zenith and horizon positions. The values d + Δd (90°) are given

for the two telescopes in Table 2. It is assumed here that the decrease

in aperture efficiency is entirely due to an increase in the RMS reflector

deviation. The alternative possibility to explain the deterioration in

the antenna characteristics by defocusing is discussed in section 5.

4. The Error Pattern

The theoretical behaviour of the error pattern of a radio telescope

caused by random deviations of its reflector has been discussed in [2],

section 3. We will adopt an RMS reflector deviation of $\sqrt{\overline{d^2}}$ = 1.8 mm, since

most of the measurements have been made at zenith distances of about 20

to 40°.

The average antenna temperature of the center part of the moon

measured during one lunation, is $\overline{T_M}$ = 114.5°K. Assuming the brightness

temperature of 210°K, one obtains the beam efficiency η_B' = 114.5/210 = 0.545,

whereas the beam efficiency measured with a point source is η_B = 0.35. The

beam efficiency of the undisturbed reflector is obtained from eqs. (12) with

(9), η_{B_o} = 0.775. Calculating the ratio

$$\left[\frac{\eta_B' - \eta_B}{\eta_{B_o} - \eta_B}\right] \approx \frac{0.195}{0.425} = 0.46$$

we notice that the left side of [2], eq. (17) can no longer be considered

to be $\ll$ 1 and hence [2], eq. (18) has to be written in the form

(15a)
$$\ell = \left[\left(\ell n \; \frac{\eta_{B_o} - \eta_B}{\eta_{B_o} - \eta_B'}\right)\right]^{1/2} \times \begin{cases} 1.094 \cdot 10^3 \; \lambda/R & |\, d \leq \lambda/12.566 \\ 1.375 \cdot 10^4 \; \sqrt{\overline{d^2}}/R & |\, d \geq \lambda/12.566 \end{cases}$$

where R, here the radius of the moon, has to be inserted in minutes of arc. Remembering that $d > \lambda/12.566$ and inserting the values for η_{B_o}, η_B and η_B', we finally obtain

(15b) $\ell = 1.20$ m

Eq. [2], 14 yields then a side lobe level of -16 dB and eq. [2], 13 yields the ratio $\Theta_e/\Theta_A = 10.3$ for the HPBW's of error and diffraction pattern. With $\Theta_A = 3.35'$ follows $\Theta_e = 34.5'$.

Two different attempts have been made to measure the power pattern of the 85-ft. telescopes. Figure 2a and b show drift curves of Taurus A through the H-plane of the two telescopes. Although the main beam is considerably broader due to the finite gaussian shape of Taurus, the figures show clearly that the side lobes are attenuated by about -14 dB, which is 2 dB less than predicted by theory.

At very short wavelengths, where the antenna temperatures of most radio sources are very low, the measurement of the power pattern becomes a real problem. It has been suggested, therefore, to use drift curves of the sun or the moon to determine main beam and first sidelobes of a radio telescope.

The theoretical problem consists in solving the antenna convolution integral, which might become rather difficult if the sidelobe level is high. In the case that the brightness distribution of the sun or the moon can be approximated by a step function and the angular diameter of the main beam and sidelobes of the antenna are so small that the problem can

be treated as a one dimensional problem, a relatively simple solution of the integral equation can be obtained.

The antenna convolution integral can be written in the form

$$T_A(\xi,\eta) = \eta_B \, T_o \int\limits_{-\infty}^{+\infty}\!\!\int d\xi' \; d\eta' \; f(\xi',\eta') \; \psi \, (\xi - \xi', \eta - \eta')$$

where η_B is an effective beam efficiency, T_o the maximum brightness temperature of the sun or the moon, $\psi(\xi,\eta)$ the brightness distribution function ($\psi_{max} = 1$) and $f(\xi,\eta)$ the unknown antenna pattern. Assuming now that the antenna pattern can be approximated by a function $f(\xi,\eta) = f_1(\xi) \, f_2(\eta)$ (which is always the case for a gaussian function) and that the distribution function depends only on one coordinate $\psi(\xi,\eta) = \psi(\xi)$ the integration in η can be performed and the convolution integral yields

(16)
$$T_A(\xi) = \eta_B T_o I(\eta) \int\limits_{-\infty}^{+\infty} d\xi' \; f_1 \, (\xi') \; \psi \, (\xi - \xi')$$

with
$$I(\eta) = \int\limits_{-\infty}^{+\infty} d\eta \; f_2(\eta)$$

Figures 3a and b show drift curves measured with the 85-ft. telescopes at $\lambda = 2.07$ cm, which can be approximated by the integral equation (16). The angular coordinate ξ describes the position of the center of the antenna beam relative to the center of the moon's disk ($\xi = \eta = 0$). The dashed curves in this figure have been calculated by convolving a gaussian antenna pattern with $\theta_A = 3.35'$ with a disk with 16' radius. The quite considerable deviation of the measured curves from the calculated curves show that either the antenna pattern deviates strongly from the gaussian approximation or the distribution of the radiation temperature of the moon deviates strongly from a disk distribution. We assume now that the moon has really a disk distribution and try to calculate the antenna pattern. Differentiating eq. (16) we obtain

(17)
$$\frac{dT_A(\xi)}{d\xi} = \eta_B T_o I(\eta) \int_{-\infty}^{+\infty} d\xi' \; f_1(\xi') \frac{d}{d\xi} \Psi (\xi - \xi')$$

$$= \eta_B T_o I(\eta) \cdot f_1(\xi)$$

considering the fact that $\frac{d}{d\xi} \Psi (\xi - \xi') = \delta(\xi - \xi')$ (Dirac-function) and
the convolution $f_1(\xi')* \; \delta(\xi - \xi') = f_1(\xi)$.

Each drift curve of the moon yields consequently two approximations
of the power pattern. The differentiated curves have merely to be nor-
malized to unity. Fig. 4a and b show the results of these calculations.
The HPBW obtained from calculating the best fitting gaussian curves agree
pretty well with the corresponding values obtained from drift curves with
the planets. The sidelobes, however, are considerably higher than would
be expected from the drift curves fig. 2a and b. This may be due to the
fact that the brightness distribution of the moon deviates from the step
function assumed in the derivation of eq. (17).

This method is of special importance for measurements of the antenna
power pattern in the mm-wave range. F. Low supplied a drift curve of the
sun through the NRAO 5-ft. telescope at a wavelength of $\lambda = 1.2$ mm (fig.
5a). Using eq. (17) we derived the main beam pattern of the 5-ft. tele-
scope shown in fig. 5b. The HPBW of the telescope, as obtained by averaging
the two sets of points obtained from the east and west limb, respectively,
yields $\Theta_A = 3.8$ min. of arc. The HPBW expected from theory would be
$\Theta_A = 3.3$ min. of arc. We believe that by averaging the results obtained
from five or ten drift curves would yield a fairly good result, since
then most of the fluctuations in the differentiated curves, which are mostly
due to noise fluctuations in the original drift curves, could be eliminated
by the averaging process.

5. The Effect of Axial Defocusing of the Antenna Feed

We call Δf_{ax} the distance between the phase center of the feed and the focal point of the paraboloidal reflector. As a result of the axial defocusing a quadratic phase error is introduced (Appendix eq. I,1).

$$(18) \qquad \psi(r) = \beta r^2 \text{ with } \beta = \frac{2\pi}{\lambda} \Delta f_{ax} (1-\cos\theta_o)$$

β has the meaning of a phase difference between central and edge ray. For not too large phase errors, the effect on the antenna characteristics can be described by a decrease in gain and aperture efficiency and an increase in HPBW. Some calculations have been made on both effects, the results of which will be shortly reviewed.

a. Gain reduction

Our calculations in Appendix I, a, lead to the following results

$$(19a) \qquad G/G_o = \left[\frac{\sin\beta/2}{\beta/2}\right]^2 \approx 1 - \beta^2/12 + \dots \text{ uniform illumination}$$

$$(19b) \qquad G/G_o = \left[\frac{\sin\beta/2}{\beta/2}\right]^4 + \frac{4}{\beta^2}\left[\frac{\sin\beta}{\beta} - 1\right]^2 \approx 1 - \frac{\beta^2}{18} +$$

$$\dots \text{ tapered illumination } (1 - r^2)$$

Both equations are plotted in fig. 6.

Bracewell [5] gives the quadratic approximation of eq. (19a). Cheng derives as a lower limit for the gain reduction [6].

$$(20) \qquad G/G_o = (1-m^2/2) \approx 1-m^2, m \ll 1$$

m is defined as the maximum phase deviation from the average phase value across the aperture plane. Hence,

$$\psi_{av} = 2\pi \int_o^1 dr\ r\ \beta r^2 \Big/ 2\pi \int_o^1 dr\ r = \beta/2 \text{ and } m = \psi_{max} - \psi_{av} = \beta/2$$

Inserting this value into eq. (20) and comparing the result with eq. (19a) shows that m has to be taken $1/\sqrt{3}$ of its value (in the case of uniform illumination) to get agreement between eqs. (19a) and (20). In the case of a tapered illumination m has to be taken $\sqrt{2/3}$ of its computed value to get agreement between eqs. (19b) and (20).

b. Beam broadening

Various computations of the beam broadening as a function of the quadratic phase error β^2, introduced by an axial feed displacement, are discussed in appendix I,b. If we use the quadratic approximation for the beam broadening

$$\theta'_A/\theta_A = 1 + a\beta^2$$

we find values for the constant a varying between 0.002 and 0.06. The numerical computation of Cheng and Moseley [7], which seems to yield the most reliable results, leads to a value of $a = 0.01$. Their computations have been made for a feed taper $(1-r^2)^2$.

If we focus the antenna with an extended radio source like the sun or the moon, we have to take into account not only the decrease of aperture efficiency in the direction of the electrical axis (as in the case of a point source) but we have to consider also the increase in the HPBW and the increase in the level of the first sidelobes which are caused by the axial defocusing. This can be clearly seen from fig. 7a and b, where focussing curves for the 85(I)-ft. telescope are shown, measured at 6 and 2.07 cm wavelength, respectively. The curves (a) have been computed from eq. (19b); the measurements with a point source agree fairly well with

these curves. In the case of the 6-cm measurements the HPBW of the tele-
scope (11 min. of arc) is about 1/3 of the diameter of the moon. Con-
sequently only a fraction of the first sidelobe of the telescope is con-
tained within the apparent diameter of the moon. The experimental result
that the relative antenna temperature of the moon decreases more slowly
with axial defocusing than the relative antenna temperature of a point
source must be mainly due to the beam broadening. The antenna temperature
of the moon is given by the relation

$$(21a) \qquad T_A = \eta_B \frac{\Omega'_s}{\Omega_m} T_M$$

The effective source angle Ω'_s becomes in this case approximately $\Omega'_s \approx \Omega_m$.
The beam efficiency can be expressed by $\eta_B = \eta_R \Omega_m / \Omega = \eta_R \Omega_m G / 4\pi$, so that
we can rewrite eq. (21a) in the form

$$(21b) \qquad T_A = \frac{\eta_R}{4\pi} \Omega_m G T_M$$

The antenna temperature of a point source decreases proportional to G. For
small phase errors we can use the quadratic approximation $G = G_o (1 - b\beta^2)$.
In the case of an extended source whose diameter is at least two times the
HPBW of the antenna, the relative antenna temperature decreases proportional
to the product $\Omega_m G$. Since $\Omega_m \sim \Theta_A^2$, we can write for the quadratic approxi-
mation $\Omega_m = \Omega_{mo}(1 + 2a\beta^2)$. Computing the product we obtain

$$(22) \qquad \Omega_m G = \Omega_{mo} G_o [1 - (b - 2a) \beta^2 - 2ab\beta^4]$$

Eq. (19b) yields for b = 0.055. From the measured change in the antenna
temperature of the moon at λ = 6-cm, we find for a = 0.018. Figure 8
shows some computed quadratic approximations of the beam broadening; the
solid curve has been derived from the observations of fig. 7a, using

for $G(\beta)$ the rigorous equation (19b). One sees that for larger phase errors the beam broadens considerably stronger than would be expected from the quadratic approximation.

Our calculations in Appendix I show that the beam broadening depends very strongly on the taper of the feed pattern. The voltage patterns of various feeds used in the measurements are shown in fig. 9, together with some convenient and often used approximations for the tapered feed patterns. The free space taper has been added to the original feed patterns.

Fig. 7b shows the same focusing curves as fig. 7a, but measured at 2.07-cm wavelength. The HPBW of the 85-ft. telescope is, in this case, only 3.35 min. of arc, so that about the first four sidelobes are contained within the apparent disk of the moon. The deviation between curve (b) (which corresponds to the 6-cm observations with the moon) and the relative change of the antenna temperature of the moon at 2.07-cm is due to the increase in the level of the first four sidelobes.

At very short wavelengths it is hard to focus an antenna with a point source, since in this wavelength region the only strong radio sources are the sun and the moon. It has been suggested, therefore, to use these sources for the antenna focusing at very short wavelengths. Our observations in fig. 7a and b show, however, that the symmetry line of the focusing curves obtained with the moon do not coincide with the focal point which is found with a point source, but lies between 0.3 and 0.5 wavelength closer to the reflector.

If the decrease in gain observed at both 85-ft. telescopes should be caused by an axial feed displacement rather than by an increase in the RMS reflector deviations, the axial defocusing should be about 1 wavelength in the case of the 85(I)-ft. telescope and about 0.3 wavelength in the case

of the 85(II)-ft. telescope. The photogrammetric survey yields a change

in the focal length of the best fitting paraboloid of about 4-cm. The

contour map representation of the reflector deviations at zenith (fig. 10a)

and at horizon (fig. 10b) reveals in addition a very strong astigmatism

of the reflector at small elevation angles.

Appendix I

Some calculations on "axial defocusing"

a) Gain reduction

We call Θ the angle between the symmetry axis of the paraboloidal reflector and a ray drawn to the point x,y on the reflector surface. It can be easily shown that the phase difference between the central ray and the ray reflected at the point x,y is proportional to $\sin \Theta$ in the case of a radial defocusing and proportional to $\cos \Theta$ in the case of an axial defocusing. Since

$$\sin \Theta \sim \frac{x}{f} - \frac{x^3}{2f^3} \; \dots$$

and

$$\cos \Theta \sim \left(\frac{x}{2f}\right)^2 - \left(\frac{x}{2f}\right)^4 \dots$$

the phase difference increases proportional to the square of the normalized distance $r = x/(D/2)$ in the case of an axial defocusing, and proportional to $ar + br^3$ in the case of a radial defocusing.

The maximum difference in path length occurs between central ray and edge ray and is in the case of axial defocusing

$$(I,1) \qquad \Delta l_{max} = \Delta f_{ax} (1 - \cos \Theta_o)$$

Δf_{ax} is the difference between the phase center of the feed and the focal point of the reflector, Θ_o is the aperture angle. The phase error across the aperture as a function of the normalized distance r is then

$$(I,2) \qquad \Psi(r) = \beta r^2 \text{ with } \beta = \frac{2\pi}{\lambda} \Delta f_{ax} (1 - \cos \Theta_o)$$

The voltage pattern of a circular aperture with the aperture field distribution $F(\rho,\varphi')$ is ([8], page 192).

$$(I,3) \qquad g(\theta,\varphi) = \int_0^{D/2} \int_0^{2\pi} F(\rho,\varphi') e^{jk\rho \sin\theta \cos(\varphi-\varphi')} \rho\, d\rho\, d\varphi'$$

Introducing the quadratic phase error we can write $F(\rho,\varphi') = A(\rho,\varphi') e^{-j\beta\rho^2}$

and obtain for the secondary pattern in the Fraunhofer region

$$(1,4a) \qquad g(\theta,\varphi) = \int_0^{D/2} \int_0^{2\pi} A(\rho,\varphi') e^{jk\rho \sin\theta \cos(\varphi-\varphi')} e^{-j\beta\rho^2} \rho\, d\rho\, d\varphi'$$

Performing the integration for the case of a constant illumination of the aperture $A(\rho,\varphi') = $ const. yields

$$(I,4b) \qquad g(u) = 2 \int_0^1 J_0(ur) e^{-j\beta r^2} r\, dr$$

with

$$u = \frac{\pi D}{\lambda} \sin\theta$$

If we are only concerned with the antenna gain in the direction of the electrical axis $(u = 0)$, we find for eq. (I,4b)

$$(I,5a) \qquad g(0,\beta) = 2 \int_0^1 e^{-j\beta r^2} r\, dr = e^{-j\beta/2} \frac{\sin(\beta/2)}{\beta/2}$$

and for the power pattern

$$(I,5b) \qquad f(0,\beta) = g(0,\beta) \cdot g^*(0,\beta) = \left[\frac{\sin(\beta/2)}{\beta/2}\right]^2 \approx 1 - \frac{\beta^2}{12}$$

This is the formula usually used to calculate the gain variation as a function of the on-axis position of the phase center of a feed in the case of constant illumination. In order to get an idea how much this relation will be changed by a tapered illumination, we assume an illumination $A(r) \approx (1 - r^2)$. (I,5a) then takes the form

$$(I,6a) \qquad g(0,\beta) = 4 \int_0^1 (1 - r^2) e^{-j\beta r^2} r\,dr = 2 \int_0^1 (1 - z)e^{-j\beta z} dz$$

$$= 2 \left[-\frac{j}{\beta} + \frac{1}{\beta^2} \left(1 - e^{-j\beta} \right) \right] = \left[\frac{\sin (\beta/2)}{\beta/2} \right]^2 + j\frac{2}{\beta} \left[\frac{\sin \beta}{\beta} - 1 \right]$$

and we obtain for the power pattern

$$(I,6b) \qquad f(0,\beta) = g(0,\beta) \cdot g^*(0,\beta) = \left[\frac{\sin (\beta/2)}{\beta/2} \right]^4 + \frac{4}{\beta^2} \left[\frac{\sin \beta}{\beta} - 1 \right]^2$$

$$\approx 1 - \frac{\beta^2}{18}$$

These results show that gain and aperture efficiency decrease more slowly in the case of a tapered illumination. Both eqs. (I,5 and 6) are shown in fig. 6.

b) Beam broadening

We consider again the simplest case of uniform illumination. But now we have to solve equation (I,4b) for the far field pattern of a circular aperture with quadratic phase error for values of the variable u at least up to the order of u_o, the value of u at the half power points of the pattern. Writing eq. (I,4b) in the form

$$(I,7a) \qquad g(u) = 2e^{-j\beta} \int_0^1 e^{j\beta(1 - r^2)} J_o(ur) \, r\,dr$$

it is possible to relate the integral

$$(I,7b) \qquad g(u)e^{j\beta} = \frac{2}{\beta} \left[U_1(\beta,u) + jU_2(\beta,u) \right]$$

to the lommel functions

(I,8) $$U_1(\beta,u) = \beta \int_0^1 J_0(ur) \cos[\beta(1-r^2)] \, rdr$$

$$U_2(\beta,u) = \beta \int_0^1 J_0(ur) \sin[\beta(1-r^2)] \, rdr$$

for which the series expansions exist

(I,9) $$U_1(\beta,u) = \frac{2\beta}{u} J_1(u) - \left(\frac{2\beta}{u}\right)^3 J_3(u) + \left(\frac{2\beta}{u}\right)^5 J_5(u)$$

$$U_2(\beta,u) = \left(\frac{2\beta}{u}\right)^2 J_2(u) - \left(\frac{2\beta}{u}\right)^4 J_4(u) + \ldots$$

And we obtain finally for the power pattern

(I,10) $$f(\beta,u) = \frac{4}{\beta^2}\left[U_1^2(\beta,u) + U_2^2(\beta,u)\right]$$

$$= 4\left[\frac{J_1(u)}{u}\right]^2 - 16\beta^2\left[\frac{2J_1(u)J_3(u)}{u^4} - \frac{J_2^2(u)}{u^4}\right] + \ldots$$

As one expects

$$f(\beta,0) = 1 - 16\beta^2 \lim_{u\to0}\left\{\frac{2J_1(u)J_3(u)-J_2^2(u)}{u^4} + \ldots\right\} = 1 - \frac{1}{12}\beta^2 + \ldots$$

and

$$f(o,u) = \left(\frac{2J_1(u)}{u}\right)^2$$

In order to calculate the HPBW of the broadened beam we have to renormalize

the power pattern

(I,11a) $$f(\beta,u) = \frac{f_0(u)}{1 - \beta^2/12} - \frac{16\beta^2}{1 - \beta^2/12}\left[\frac{2J_1(u)J_3(u)}{u^4} - \frac{J_2^2(u)}{u^4}\right]$$

Expanding the Bessel functions and breaking off after the quadratic term

yields after some calculation

$$(I,11b) \qquad f(\beta,u) = \frac{f_o(u)}{1 - \beta^2/12} - \frac{\beta^2/12}{1 - \beta^2/12} \left[1 - \frac{u^2}{4} - \frac{u^4}{96} \right]$$

We call u_1 the normalized angular coordinate, at which the power pattern of the broadened beam has dropped to 1/2, and find the following equation for u_1, neglecting the term with u_1^4.

$$f_o(u_1) = \frac{1}{2} \left\{ 1 + \frac{\beta^2}{12} \left(1 - \frac{u_1^2}{4} \right) \right\}$$

Inserting here the usual gaussian approximation $f_o(u) = \exp \left\{ - \frac{u^2}{(1.2\ u_o)^2} \right\}$

with u_o the normalized angular coordinate corresponding to the HPBW of the undisturbed main beam, we can calculate the main beam solid angle

$$(I,12a) \qquad \Omega_m' = \Omega_m \left(1 + 0.1\beta^2 - 0.16 \frac{\beta^4}{12} \right)$$

and

$$(I,12b) \qquad \Theta_A' = \Theta_A (1 + 0.05\beta^2 - 0.038\beta^4)$$

Another possibility to calculate approximately the increase in HPBW consists in expanding the antenna pattern $f(u,\beta)$ in a Taylor series. Let $u_1 = u_o + \Delta u$ be the argument at which $f(u_1,\beta) = 1/2$. We then calculate Δu by solving the equation

$$(I,13) \qquad f(u_1) = 1/2 = f(u_o) + \Delta u\ f'(u_o) + \frac{(\Delta u)^2}{2} \cdot f''(u_o) + \dots$$

This leads to

$$(I,14a) \qquad u_1/u_o \approx 1 + 0.002\ \beta^2$$

if only $f'(u_o)$ is considered, and to

(I,14b) $u_1/u_o \approx 1 + 0.003 \ \beta^2$

if $f''(u_o)$ is considered also. Comparison with our experimental results shows that the beam broadening conforming to eqs. 14 is too small, an effect which is probably due to the slow convergence of the Taylor expansion.

Cheng [6] gives an upper limit for Δu

(I,15) $$\Delta u < \frac{m^2}{2} \left[\frac{g_o(u)}{-\frac{d}{du} g_o(u)} \right] u_o$$

Inserting for the voltage pattern the gaussian approximation $g(u) = \sqrt{f(u)} = \exp \{- u^2/2 \ (1.2u_o)^2\}$, we obtain $\Delta u < 0.72 \ m^2 u_o$. The discussion of eq. (20) suggests to replace m by $m/\sqrt{3}$ for the case of constant illumination and by $m\sqrt{2}/3$ in the case of a $(1 - r^2)$ tapered feed pattern. We find in the case of constant illumination:

(I,16a) $u_1/u_o = \theta_A'/\theta_A = 1 + 0.060 \ \beta^2$ for a gaussian main beam

and

(I,16b) $u_1/u_o = \theta_A'/\theta_A = 1 + 0.057 \ \beta^2$ for a Bessel function representation of the main beam

and in the case of a $(1 - r^2)$ taper

(I,17a) $u_1/u_o = \theta_A'/\theta_A = 1 + 0.040 \ \beta^2$ gaussian main beam

and

(I,17b) $u_1/u_o = \theta_A'/\theta_A = 1 + 0.038 \ \beta^2$ Bessel function representation

Silver ([8], page 189) gives an expression for the voltage pattern in the presence of a quadratic phase error, which is written in the form of a series expansion of derivatives of $g_o(u)$, the voltage pattern of the focussed antenna.

$$(I,18) \qquad g(u) = \sum_{n=0}^{\infty} \frac{1}{j^n} \frac{\beta^n}{n!} \frac{d^{(2n)}}{du^{2n}} \left[g_o(u) \right]$$

Breaking off the series after the third term* we get

$$(I,19a) \qquad g(u) = g_o(u) - j\beta \, g_o^{(2)}(u) - \frac{1}{2} \beta^2 g_o^{(4)}(u)$$

and consequently the power pattern

$$(I,19b) \qquad f(u) = g_o^2(u) - \beta^2 \left\{ g_o(u) g_o^{(4)}(u) - \left[g_o^{(2)}(u) \right]^2 \right\}$$

It has to be borne in mind, however, that the formula is only valid for a linear aperture (including a square aperture which can be treated in a similar way).

As an experimental result we find a beam broadening which can be approximated by

$$(I,20) \qquad \theta'_A/\theta_A \approx 1 + 0.02 \, \beta^2$$

This shows that the analytically derived results yield either too high or too small values for the beam broadening. A natural step is to compute better approximations using numerical methods. Cheng and Moseley [7] considered the necessary defocusing of an antenna in order to obtain far field

---

*Silver included in his formula only the second derivative, which leads to a wrong approximation. We are indebted to Dr. J. Ruze to have pointed out to us in a private communication that the fourth derivative has to be included.

characteristics in the Fresnel zone. They calculate for a feed pattern

taper $(1 - r^2)^2$ a beam broadening, which can be approximately represented

by

(I,20) $\theta'_A/\theta_A = 1 + 0.01 \beta^2$

The curve of this equation is also drawn in fig. 8.

References

[1]   Mezger, P.G., Application of the Antenna Tolerance Theory to the
      NRAO 85-ft. and 300-ft. Telescopes. NRAO Electronics
      Division Internal Report No. 17, August 1963.

[2]   Baars, J.W.M. and P. G. Mezger. The Characteristics of the 300-ft.
      Telescope at 10-cm Wavelength. NRAO Electronics Division
      Internal Report No. 30, May 1964.

[3]   Baars, J.W.M. and P. G. Mezger. The Brightness Temperature Dis-
      tribution of the Strongest Radio Sources at 10-cm Wavelength
      Measured with the NRAO 300-ft. Telescope. NRAO Internal
      Report, April 1964.

[4]   Baars, J.W.M., P. G. Mezger and H. Wendker. The Absolute Spectra
      of the Strongest Non-thermal Radiosources in the Wavelength
      Region Between 1 Meter and 2-cm. Paper presented at the
      AAS Meeting in Flagstaff, June 1964.

[5]   Bracewell, R. N. Radio Astronomy Techniques. In Handbuch der Physik,
      Vol. 54, Springer, 1962.

[6]   Cheng, D. K. Effect of Arbitrary Phase Errors on the Gain and Beam-
      width Characteristics of Radiation Pattern. IRE Trans.
      Ant. and Prop. 3, (1955) 145.

[7]   Cheng, D. K. and S. T. Moseley, On-Axis Characteristics of the Para-
      boloidal Reflector. IRE Trans. Ant. and Prop. 3, (1955) 214.

[8]   Silver, S. Microwave Antenna Theory and Design. M.I.T. Rad. Lab.
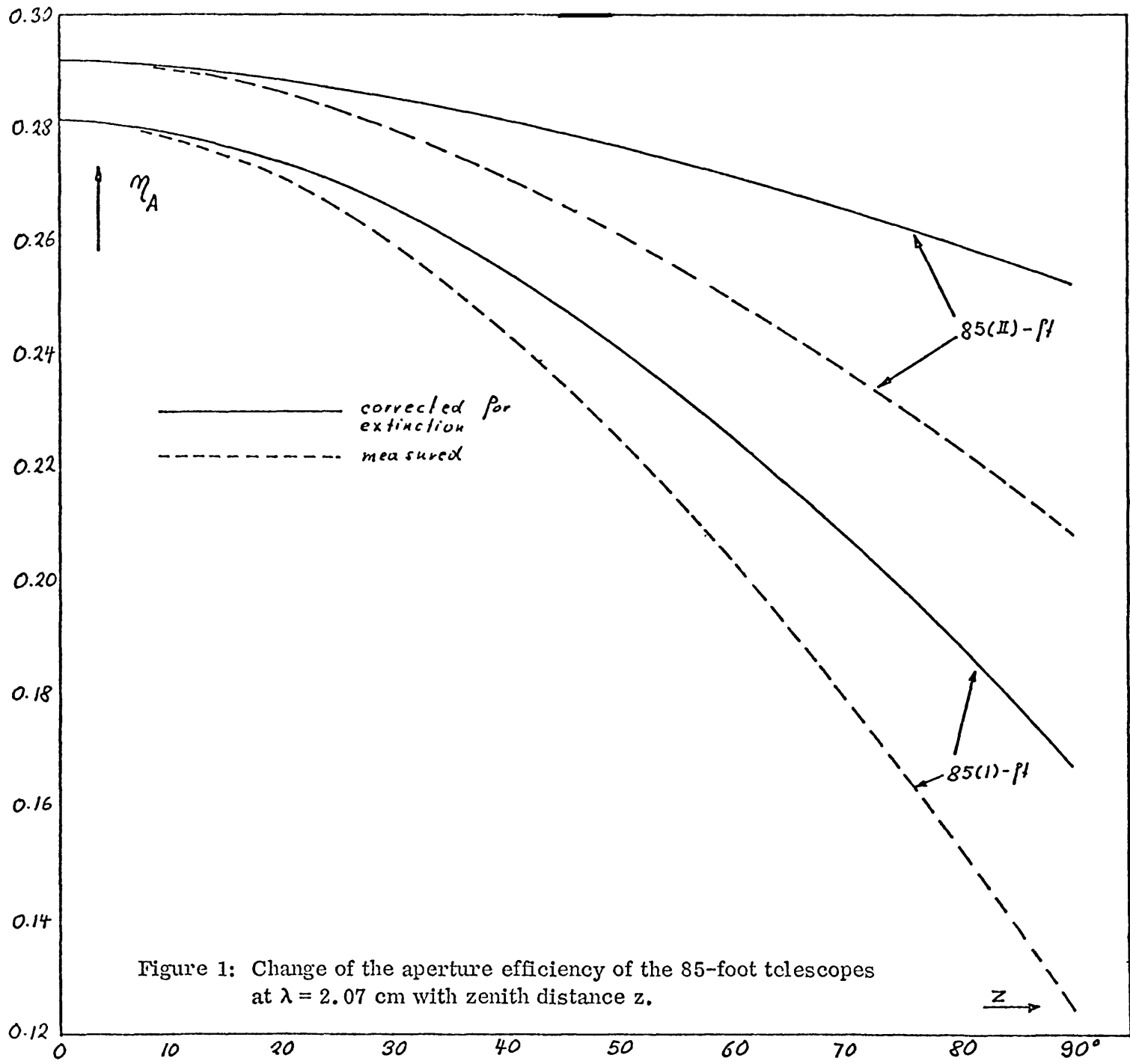   Series, Vol. 12.

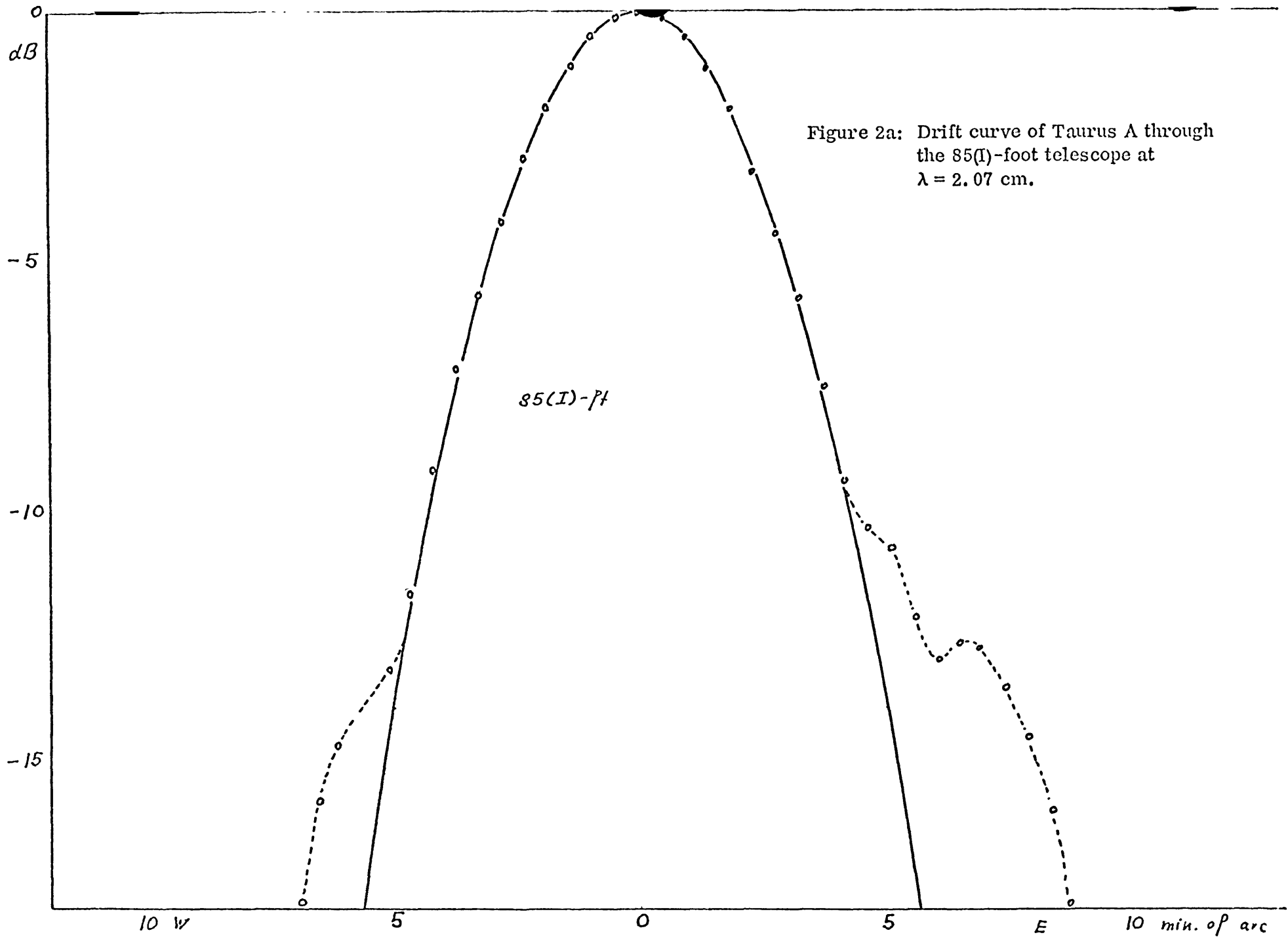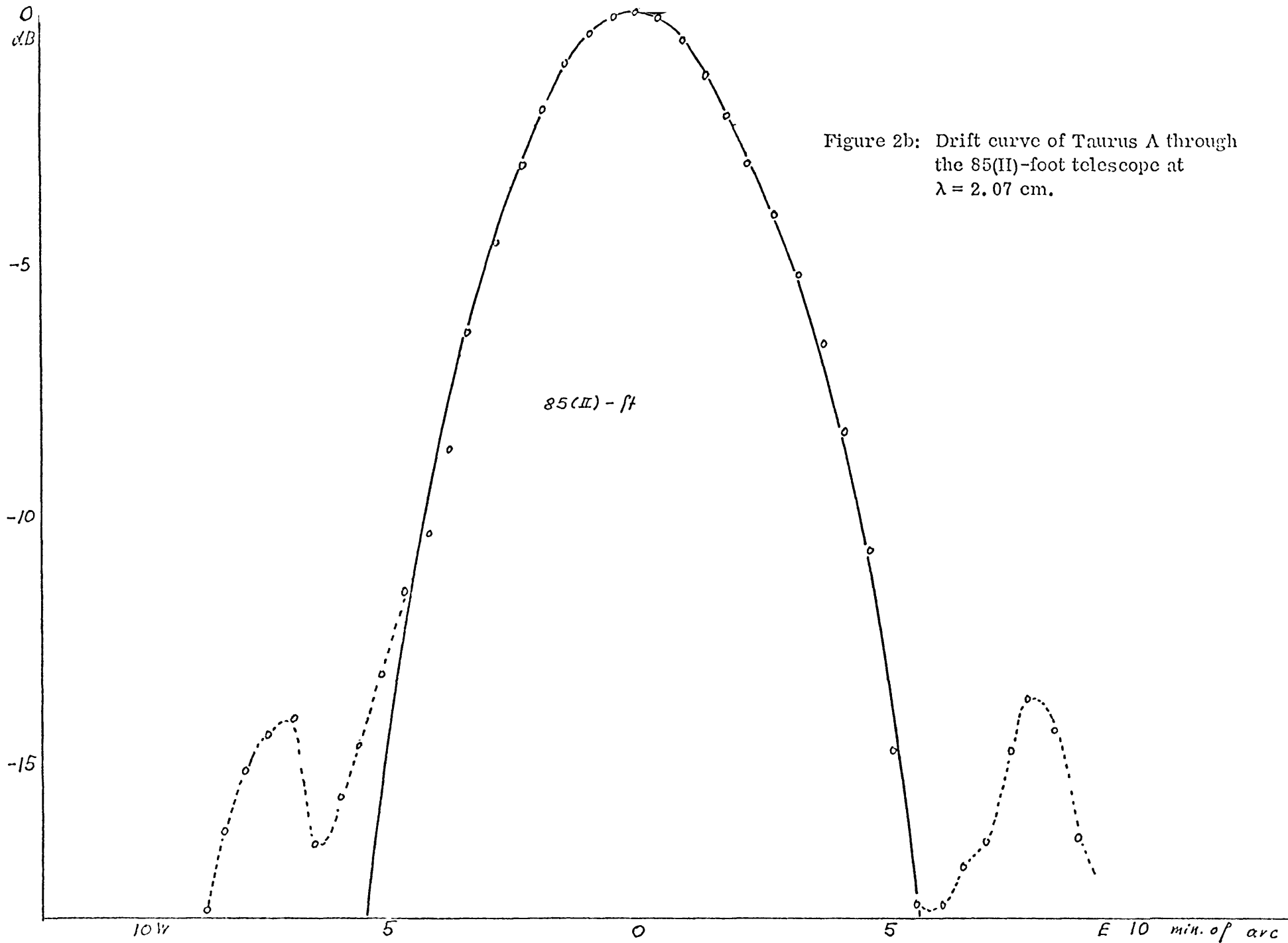Figure 1: Change of the aperture efficiency of the 85-foot telescopes at λ = 2. 07 cm with zenith distance z.

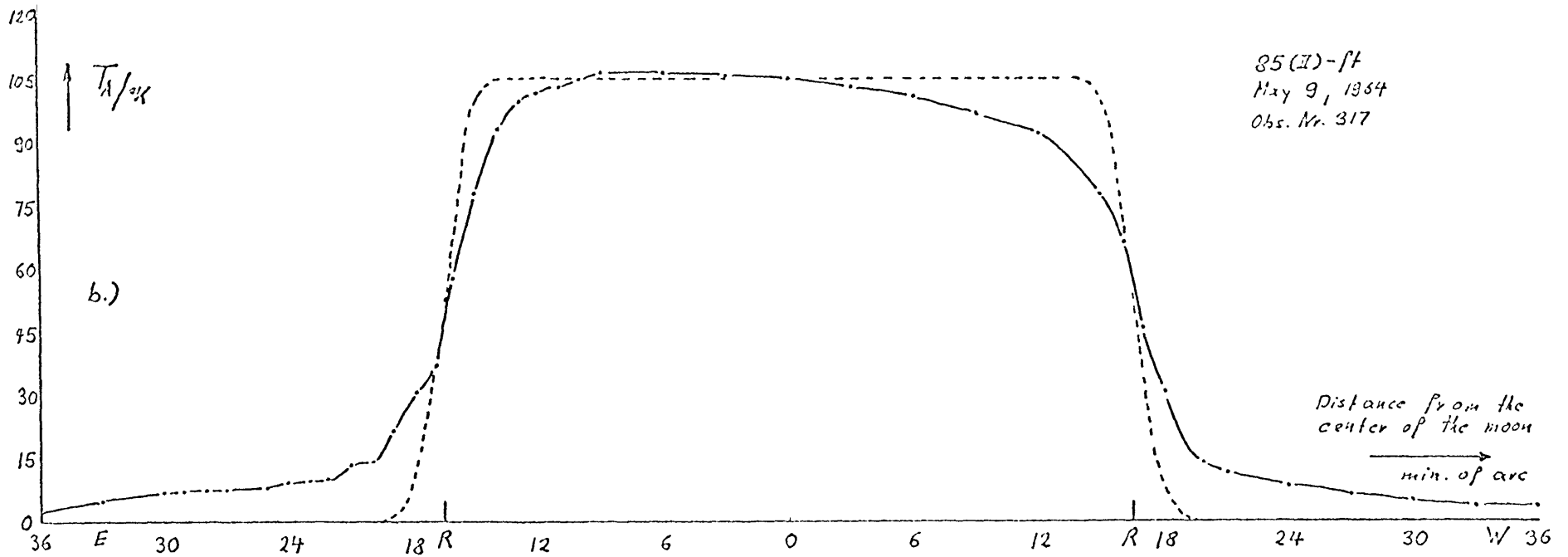Figure 2a: Drift curve of Taurus A through the 85(I)-foot telescope at λ = 2.07 cm.

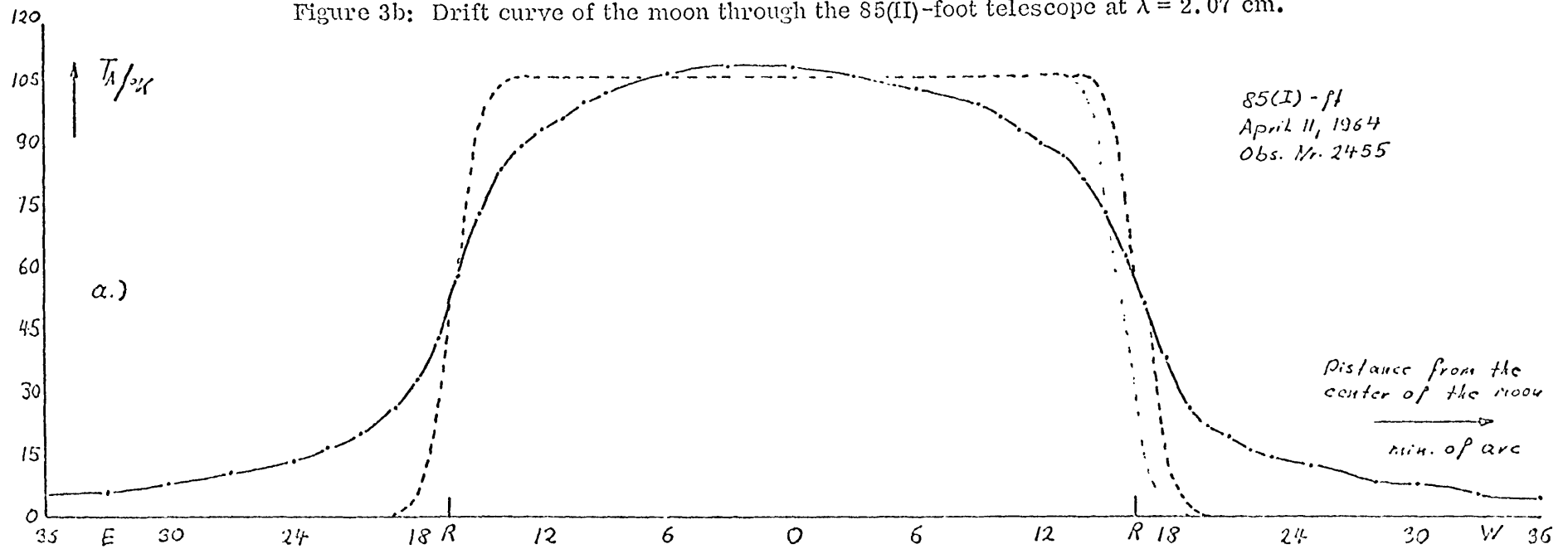Figure 2b: Drift curve of Taurus A through the 85(II)-foot telescope at λ = 2.07 cm.

85(II) - ft

10 W   5   0   5   E   10   min. of arc

Figure 3b: Drift curve of the moon through the 85(II)-foot telescope at $\lambda = 2.07$ cm.

Figure 3a: Drift curve of the moon through the 85(I)-foot telescope at $\lambda = 2.07$ cm.
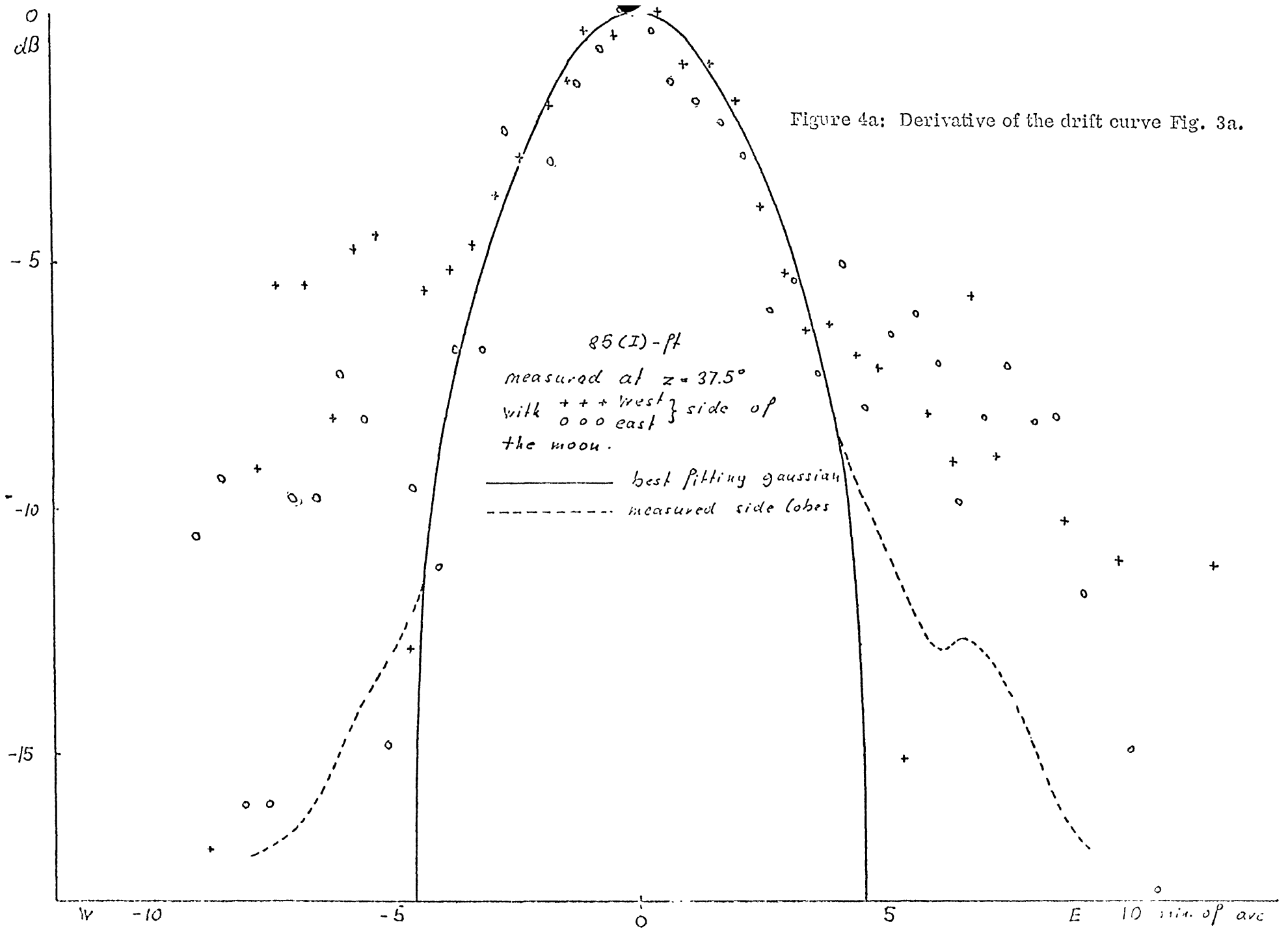
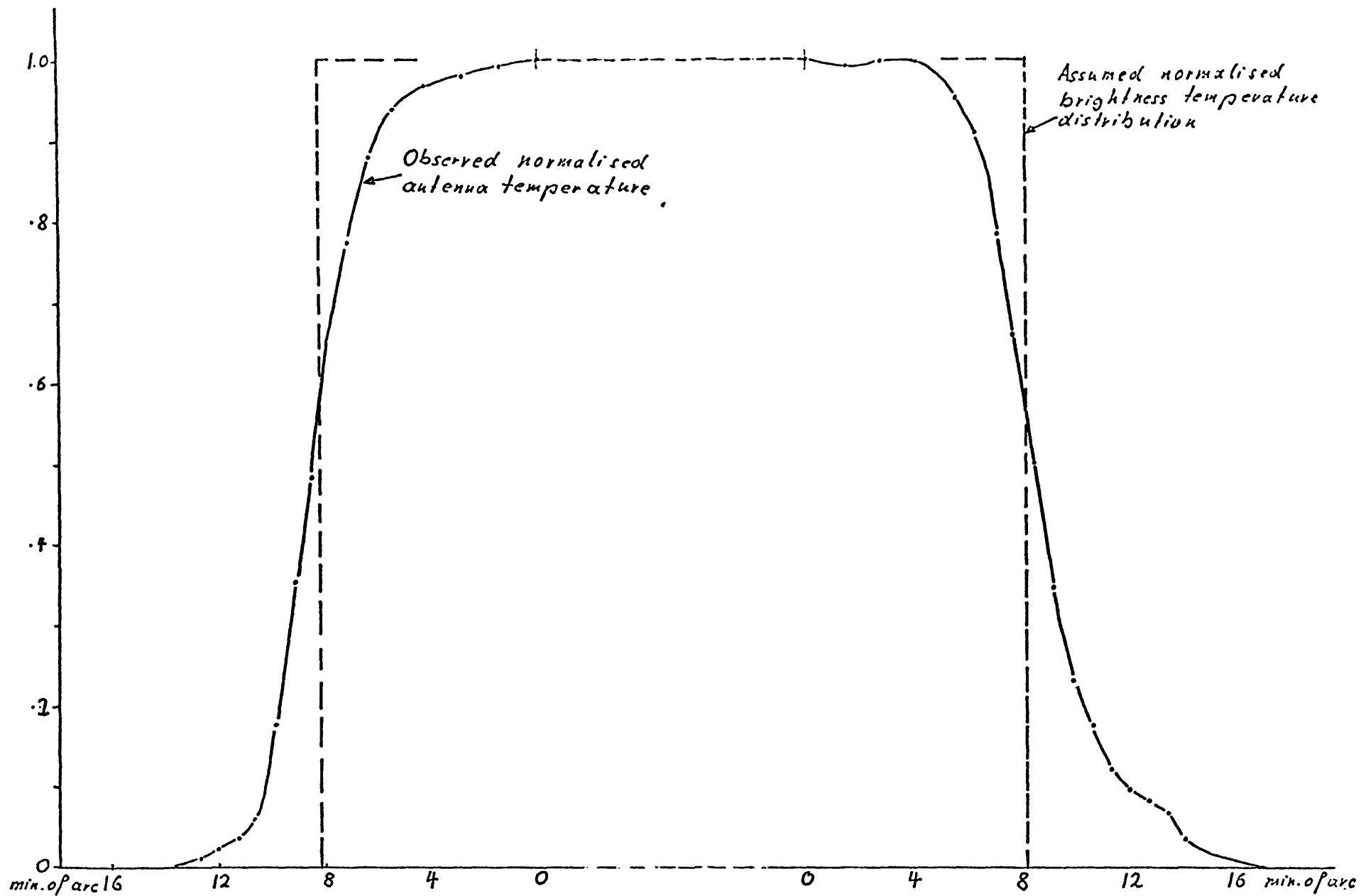Figure 4a: Derivative of the drift curve Fig. 3a.

85 (I) - ft

measured at z = 37.5°

with +++ west } side of
     ooo east } side of
the moon.

———————— best fitting gaussian
- - - - - - measured side lobes

W   -10   -5   0   5   E   10   min of arc

Figure 5a: Drift curve of the sun through the 5-foot telescope at $\lambda = 1.2$ mm

Figure 5b: Derivative of the
drift curve Fig. 5a.

o West side of the sun
+ East
$\lambda = 1.2\ mm$

5-ft-telescope

——————— best fitting gaussian
- - - - - - side lobes

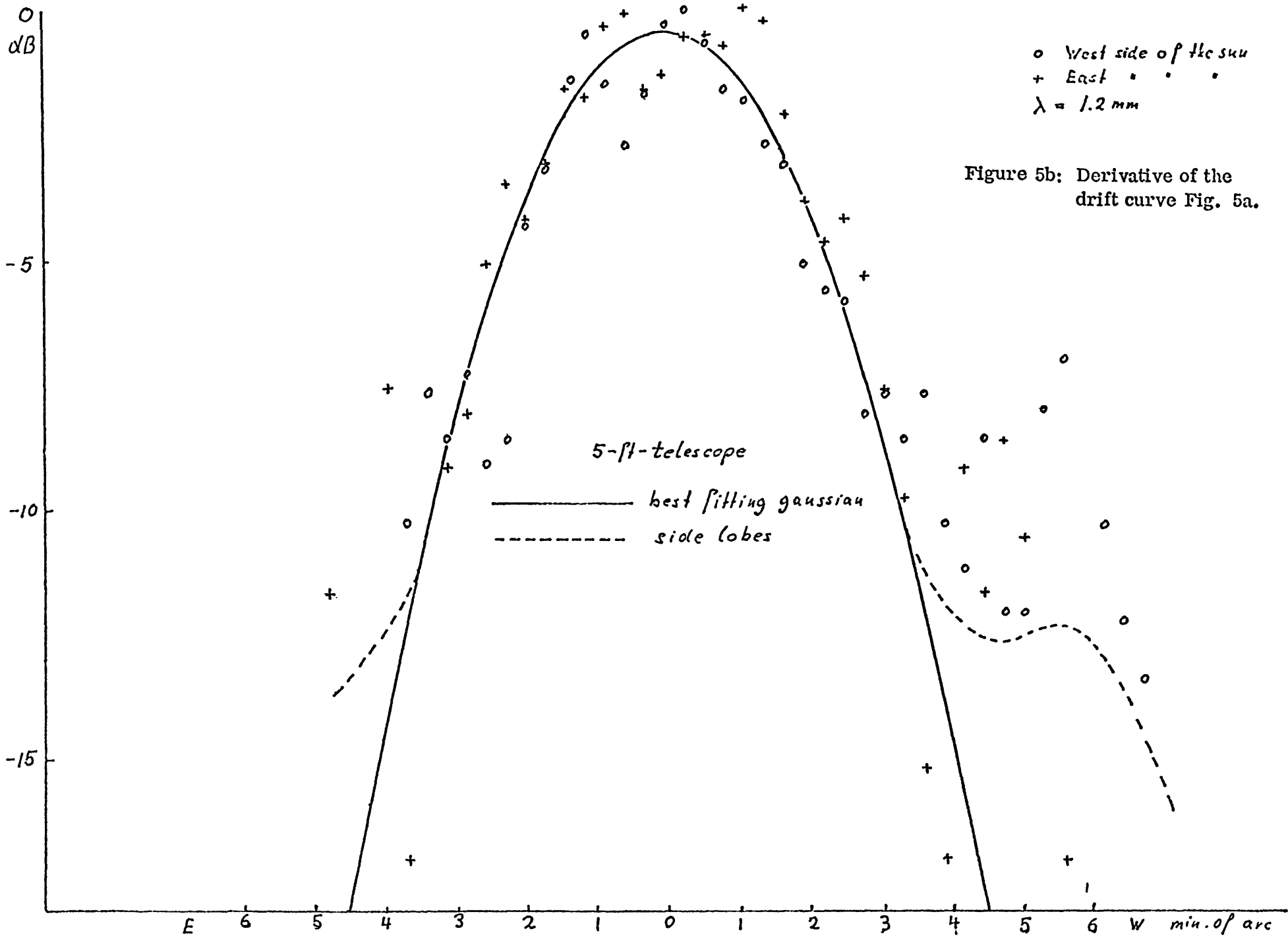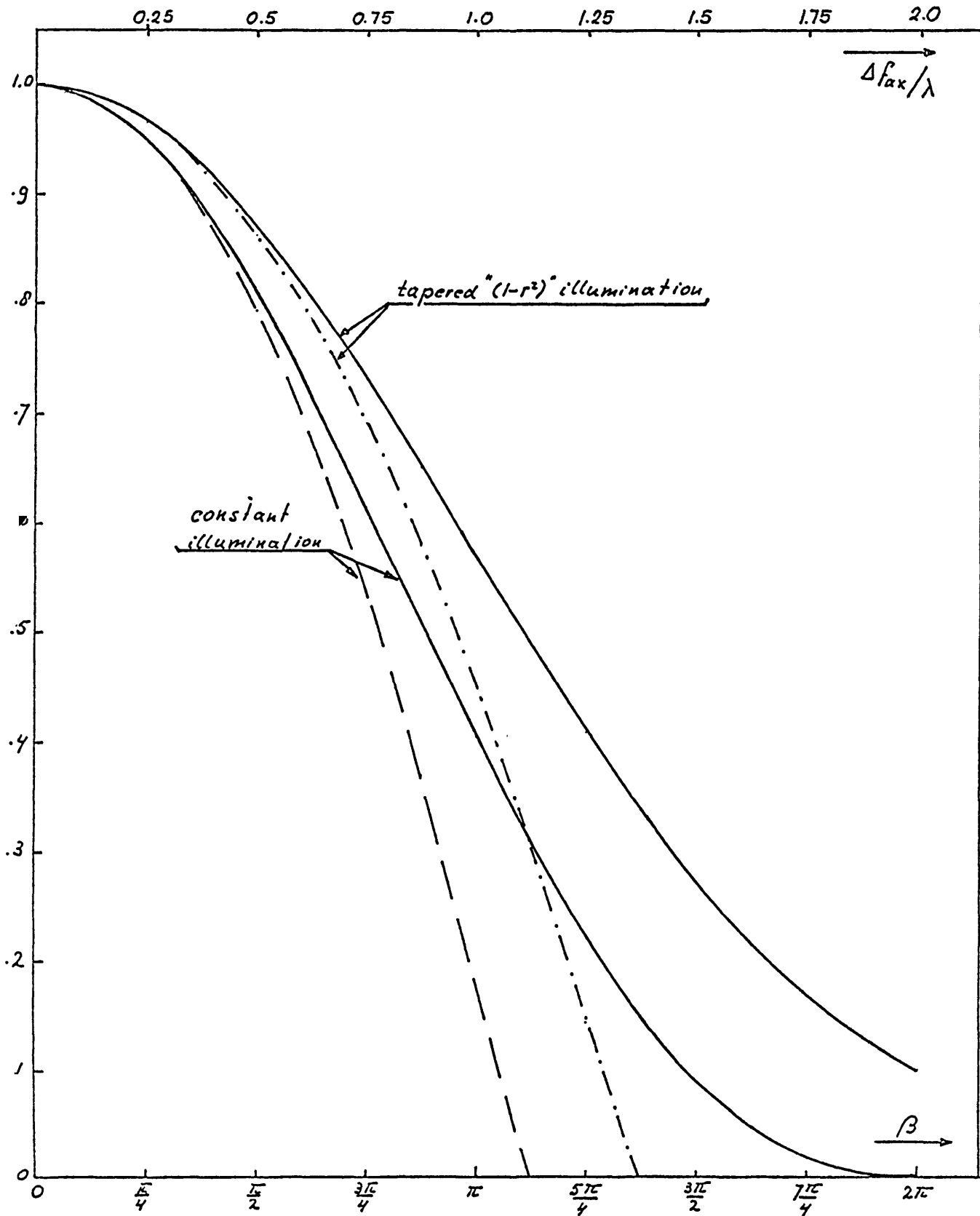dB

-5
-10
-15

E 6 5 4 3 2 1 0 1 2 3 4 5 6 W min. of arc

Figure 6: Relative change or gain and aperture efficiency as a function of the phase error β introduced by an axial defocusing. The $\Delta f_{ax}/\lambda$ scale is valid for a F/D ratio of 0.42. The dashed and dash-dotted curves, respectively, are the quadratic approximation of the rigorous functions.
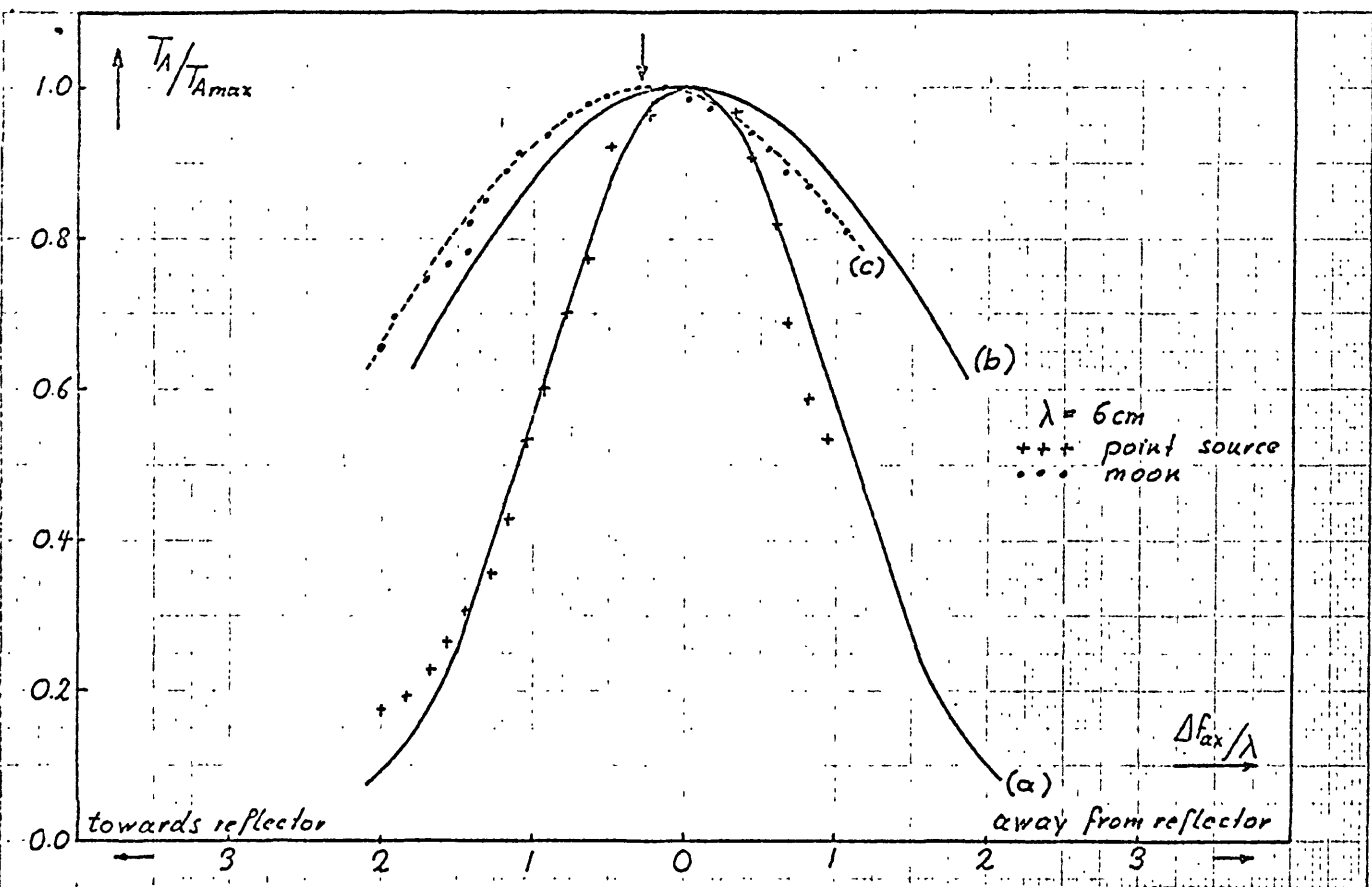
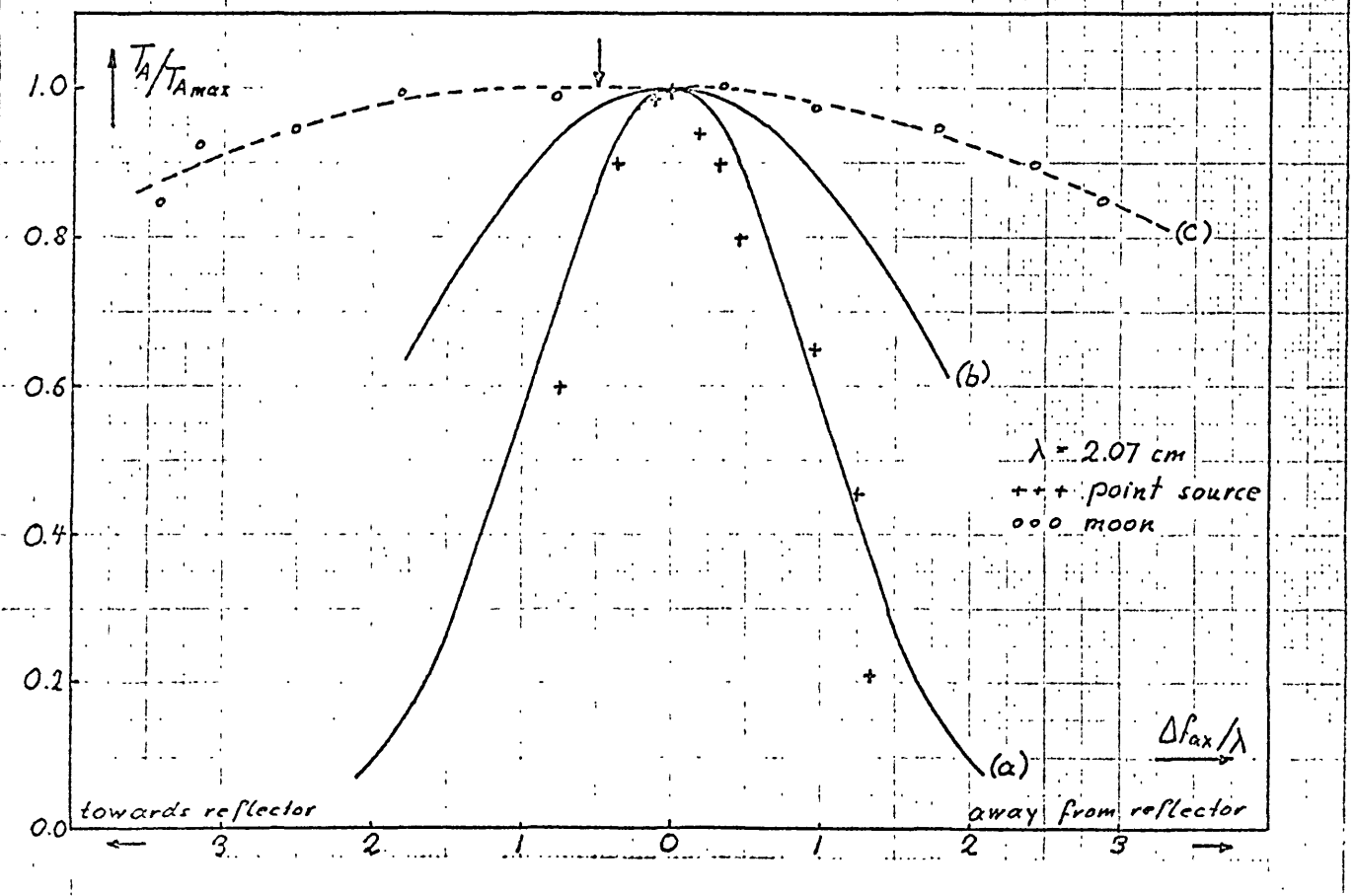Figure 7a: Focusing curves, measured with 85(I)-foot telescope at 6 cm wavelength.
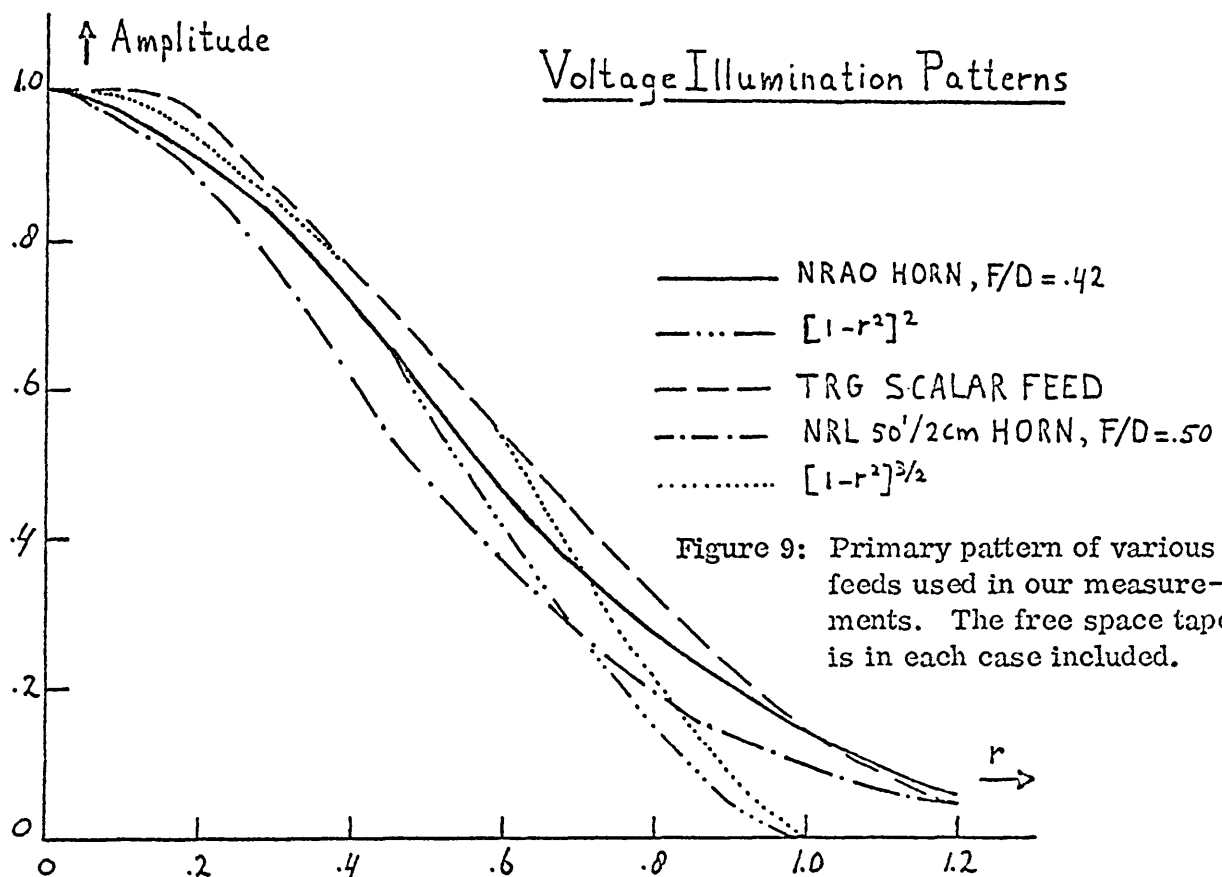

Figure 7b: Focusing curves, measured with the 85(I)-foot telescope at $\lambda = 2.07$ cm.

Beam broadening as function of axial defocusing.

measured
$[1 + 0.018\beta^2]$
$[1 + 0.01\,\beta^2]$
$[1 + 0.04\beta^2]$

Figure 8: Beam broadening as a function of the phase error β introduced by an axial defocusing. The $\Delta f_{ax}/\lambda$ scale is valid for a F/D ratio of 0.42.

Voltage Illumination Patterns

—— NRAO HORN, F/D = .42
—··— $[1-r^2]^2$
— — TRG SCALAR FEED
—·—·— NRL 50'/2cm HORN, F/D = .50
·········· $[1-r^2]^{3/2}$

Figure 9: Primary pattern of various feeds used in our measurements. The free space taper is in each case included.
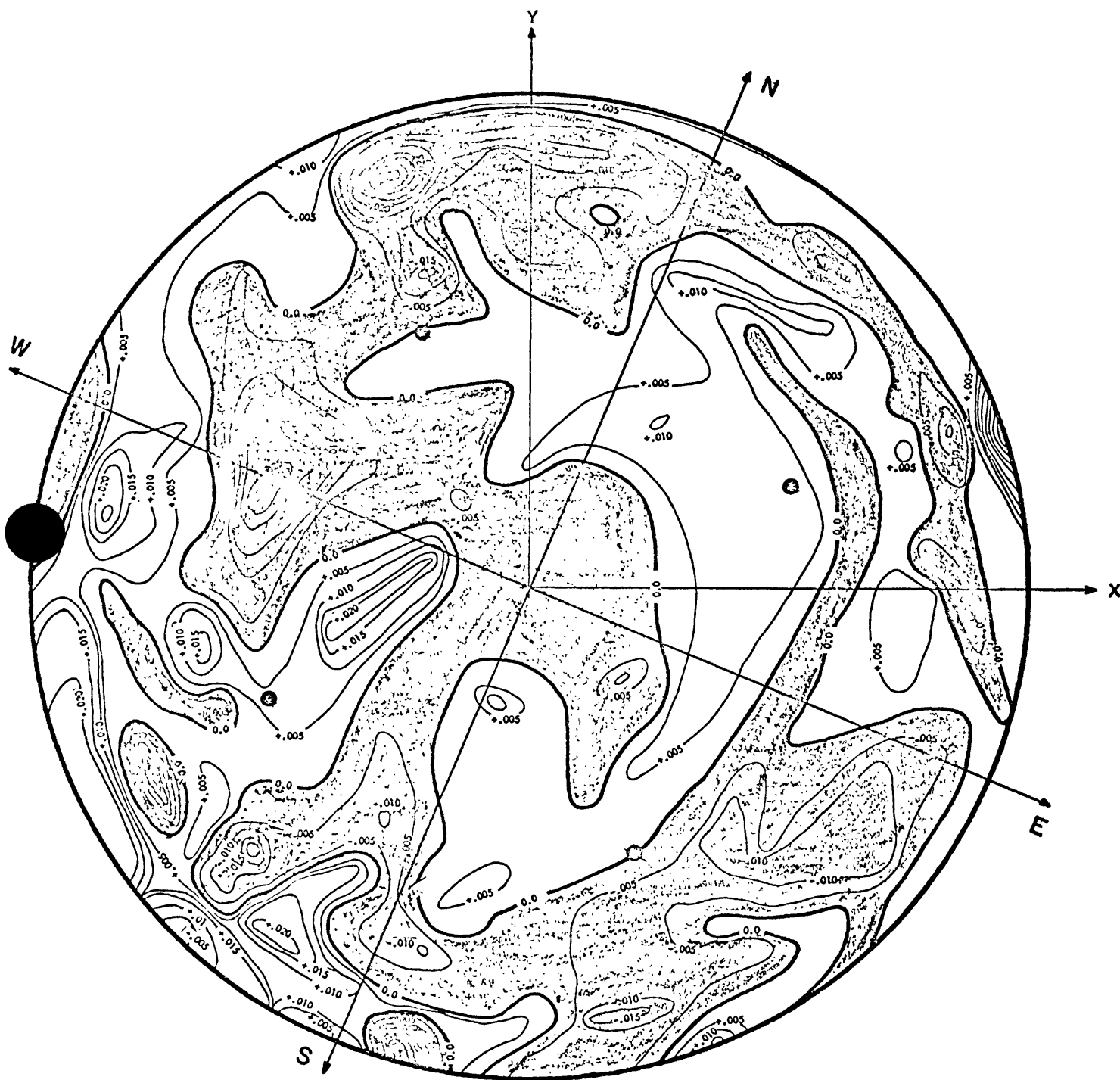
Figure 10a: Contour map representation of the 85(I)-foot reflector at z = 0°.
One contour interval ≙ 1.53 mm.